Bulletin of the Seismological Society of America, 90, 2, pp. 401–413, April 2000

Seismic Wave Propagation and Scattering in Heterogeneous Crustal Waveguides Using Screen Propagators: I SH Waves

by Ru-Shan Wu, Shengwen Jin, and Xiao-Bi Xie

Abstract The great advantages of one-way propagation methods, such as the generalized screen propagators (GSP) method, are the fast speed of computation, often several orders of magnitude faster than the full-wave finite difference and finite element methods, and the huge savings in internal memory. In this article, a half-space GSP is formulated for the *SH* half-space problem. Two versions of the half-space GSP are derived: the wide-angle pseudo-screen and the phase-screen. The Moho discontinuity is treated as parameter perturbations from the crustal background. The validity and limitations of this treatment are discussed. It is shown that half-space screen propagators can accurately propagate guided crustal waves that are composed of small-angle waves with respect to the horizontal direction. Comparisons of numerical results with a wavenumber integration method for flat crustal models and a finite difference algorithm for heterogeneous models show excellent agreements. For a model with propagation distance of 250 km, dominant frequency at 0.5 Hz, the GSP method is about 300 times faster than a finite difference algorithm with a similar accuracy. These comparisons demonstrate the accuracy and efficiency of the method. We apply our method to simulate regional wave propagation in different types of complex crustal waveguides including those with small-scale random heterogeneities. The influence of these heterogeneities on Lg amplitude attenuation and Lg coda formation is significant.

Introduction

The study of path effects of complex structure and heterogeneities on the excitation and propagation of regional phases in different areas remains critical for many seismological problems, such as the study of crustal structures and the discrimination and yield estimation for low-yield nuclear test monitoring. An ideal numerical method for investigating regional wave propagation should have the capabilities to deal with crustal models that include horizontal and vertical variations with scales from geological boundaries to small scatterers, including random heterogeneities, as well as handling 3D Q structures. For the purpose of monitoring the Comprehensive Test Ban Treaty (CTBT) at regional distances, simulation algorithms are desirable for generating synthetic waveforms for high frequencies up to 25 Hz at distances greater than 1000 km.

Substantial efforts have been made in modeling regional wave propagation. Methods based on layered earth models, such as the reflectivity and mode summation methods (e.g., Kennett, 1989, 1990; Maupin, 1989; Campillo, 1990; Campillo and Paul, 1992; Campillo *et al.*, 1993; Gibson and Campillo, 1994) have very high efficiency and can be applied to relatively high frequencies, but they can be used only for very simplified cases with layered or smoothly varying layered models. Modeling techniques that can treat realistic 3D heterogenous media rather than smoothly varying layered media are needed to test and study many observations and hypotheses. Sudden changes of crustal thickness, strong lateral variations, and irregular 3D heterogeneities are among the problems requiring new modeling methods. As pointed out by Campillo *et al.* (1993), actual Lg amplitudes were reduced more than 10 times for paths passing through an anomalous zone on the east side of the Alpine range, while the modeling results using existing methods (including the effect of known large-scale lateral structural variation) only account for 20–30% of the amplitude reduction. Other mechanisms such as the scattering and attenuation by small-scale heterogeneities must be taken into account.

Kennett (1984, 1998; Maupin and Kennett, 1987) developed a coupled mode method for calculating guided seismic waves in horizontally varying structures. The method works well for relatively low frequency waves in moderately heterogeneous models. However, the implementation of the method for high frequency 3D models still requires formidable computational efforts.

An alternative and flexible approach has been developed

by Kennett (1986), Bostock and Kennett (1990), Kennett *et al.* (1990) using ray diagrams to study Lg waves when acrossing structural boundaries. The method agrees well with modal calculations and can be applied to surface topography, 3D crustal structures, and other cases. However, the method cannot provide information on wave phenomena for complicated waveguides.

Finite-difference methods (e.g., Xie and Lay, 1994; Goldstein *et al.*, 1996; Jih, 1996) and pseudo-spectral methods (e.g., Kosloff *et al.*, 1990; Orrey *et al.*, 1996; Schatzman, 1996; Furumura and Kennett, 1997) are general numerical methods. Theoretically they can deal with arbitrarily heterogenous media. However, the capability of present-day computers usually restricts them to short propagation ranges and relatively low frequencies, which prevents them from being applied to more realistic cases.

Recently, the generalized screen method has been introduced into seismic wave simulations and applied to the problems of both exploration and theoretical seismology. The generalized screen method is based on the one-way wave equation and the one-return approximation. The one-way wave propagator GSP (generalized screen propagator) neglects backscattered waves, but correctly handles all the forward multiple-scattering effects (e.g., focusing/defocusing, diffraction, interference, and conversion between different wave types). The one-return approximation is also called the de Wolf approximation (de Wolf, 1971, 1985), which neglects the reverberation between screens and can simulate multiple-forescattering-single-backscattering (MFSB). Significant progress has been made on the development of an elastic complex screen (ECS) method for modeling elastic wave propagation and scattering in arbitrarily complicated structures (Wu, 1994, 1996; Xie and Wu, 1995; Wild and Hudson, 1997). The method is two to three orders of magnitude faster than the elastic finite difference method for medium-size 3D problem. The screen method has been successfully used in forward modeling (Wu, 1994; Xie and Wu 1995, 1996; Wu and Huang, 1995; de Hoop et al., 1999) and as a backpropagator for seismic wave imaging/migration in both acoustic and elastic media (e.g., Wu and Xie 1994; Huang and Wu 1996; Huang and Fehler, 1998; Huang *et al.*, 1999a, 1999b). In the crustal waveguide environment, the major wave energy is carried by forward propagating waves, including forward scattered waves, and therefore the neglect of backscattered waves does not change the main features of regional waves in most cases. By neglecting backscattering in the theory, the method becomes a forward marching algorithm in which the next step of propagation depends only on the present values of the wave field in a transverse cross section and the heterogeneities between the two cross sections. The saving of computing time and storage is enormous and makes it a viable method for large 3D elastic wave propagation problems. For wave propagation in heterogeneous crustal waveguides, however, the free surface and the sharp Moho discontinuity problems have to be solved and tested for the screen propagators.

As the first step, in this article we treat the two-dimensional SH problem for heterogeneous crustal waveguides. We first derive the wide-angle pseudo-screen formulas for one-way *SH* waves in a half space. Then a phase-screen algorithm is obtained under the small-angle forward scattering approximation. The Moho discontinuity is treated as parameter perturbations from the crustal background. The validity and limitations of this treatment are discussed. We then compare the simulation results of the method with those from wavenumber integration and finite difference methods. For a flat crustal model, for which the wavenumber integration (WI) method (reflectivity method) is considered accurate, our result shows excellent agreement with the WI method. For a heterogeneous crustal model with propagation distance of 250 km and dominant frequency of 0.5 Hz, the GSP method is about 300 times faster than a finite-difference algorithm (Xie and Lay, 1994) with a similar accuracy. These comparisons demonstrate the accuracy and efficiency of the half-space GSP method. We next apply our method to regional wave propagation in different types of complex crustal waveguides including those with small-scale random heterogeneities. The influence of these heterogeneities on Lg amplitude attenuation and Lg coda formation are shown to be significant.

Theory

First we derive the wide-angle screen formula for the 2D *SH* wave one-way propagation in an elastic half space. The equation of motion in a linear, heterogeneous elastic medium can be written as (Aki and Richards, 1980)

$$-\omega^2\rho(\mathbf{r})\mathbf{u}(\mathbf{r}) = \nabla\cdot\sigma(\mathbf{r}) \tag{1}$$

where ω is the frequency, $\mathbf{r} = (x, z)$ is a 2D position vector, $\mathbf{u}$ is the displacement vector, σ is the stress tensor (dyadic) and ρ is the density of the medium. Here we assume no body force exists in the medium. For an isotropic 2D elastic medium, the *SH* and the *P-SV* waves are decoupled. In this article we treat only the *SH* problem to demonstrate the applicability of the screen propagators to crustal waveguide problems.

General Wide-Angle Formulation

For a 2D *SH* problem, only the y-component of the displacement field exists and the divergence of the stress tensor can be simplified into

$$\begin{aligned}\nabla\cdot\sigma(\mathbf{r}) &= \nabla\cdot(\mu\nabla u)\\ &= \frac{\partial}{\partial x}\left[\mu(\mathbf{r})\,\frac{\partial}{\partial x}\,u\right] + \frac{\partial}{\partial z}\left[\mu(\mathbf{r})\,\frac{\partial}{\partial z}\,u\right]\end{aligned} \tag{2}$$

where $u = u_y$, ∇ is the 2D gradient operator, and μ is the

shear rigidity. We decompose the parameters of the elastic medium and the total wave field into

$$\begin{aligned} \rho &= \rho_0 + \delta\rho \\ \mu &= \mu_0 + \delta\mu \\ u &= u^0 + U \end{aligned} \tag{3}$$

where ρ_0 and μ_0 are the parameters of the background medium, $\delta\rho$ and $\delta\mu$ are the corresponding perturbations, u^0 is the primary field, and U is the scattered field. Then the *SH* wave equation can be rewritten as

$$\mu_0 \nabla^2 u + \omega^2 \rho_0 u = -[\omega^2 \delta\rho u + \nabla \cdot \delta\mu \nabla u], \tag{4}$$

or

$$(\nabla^2 + k^2) u(\mathbf{r}) = -k^2 F(\mathbf{r}) u(\mathbf{r}), \tag{5}$$

where $k = \omega/v$ is the wavenumber in the background medium and v is the background S-wave velocity defined by

$$v = \sqrt{\mu_0/\rho_0} \tag{6}$$

In the right hand side of (5), $F(\mathbf{r})$ is a perturbation operator

$$F(\mathbf{r}) = \varepsilon_\rho(\mathbf{r}) + \frac{1}{k^2} \nabla \cdot \varepsilon_\mu \nabla, \tag{7}$$

with

$$\varepsilon_\rho(\mathbf{r}) = \frac{\delta\rho(\mathbf{r})}{\rho_0}, \tag{8}$$

$$\varepsilon_\mu(\mathbf{r}) = \frac{\delta\mu(\mathbf{r})}{\mu_0}. \tag{9}$$

Equation (5) is a scalar Helmholtz equation. With a half-space scalar Green's function g^h, the scattered field U can be written as

$$U(\mathbf{r}_1) = k^2 \int_V d^2\mathbf{r} g^h(\mathbf{r}_1; \mathbf{r}) F(\mathbf{r}) u(\mathbf{r}), \tag{10}$$

where the 2D volume integration is over the volume V including all the heterogeneities in the modeling space. Using the Gauss divergence theorem equation (10) reduces to (cf. Wu, 1994)

$$U(\mathbf{r}_1) = k^2 \int_v d^2\mathbf{r} \{ g^h(\mathbf{r}_1; \mathbf{r}) \varepsilon_\rho(\mathbf{r}) u(\mathbf{r}) - \frac{1}{k^2} \nabla g^h(\mathbf{r}_1; \mathbf{r}) \cdot \varepsilon_\mu(\mathbf{r}) \nabla u(\mathbf{r}) \} \tag{11}$$

Under the forward-scattering approximation, or more generally the MFSB approximation (de Wolf, 1971, 1985; Wu and Huang 1995; Wu, 1996), the total field, and Green's function under the integration in equation (11) can be replaced by their forward-scattering approximated counterparts, and the field can be calculated by a one-way marching algorithm along the x-direction using a dual domain technique. We will derive in the following the dual domain expressions of the marching algorithm for the heterogeneous half-space case.

For each step of the marching algorithm under the forward-scattering approximation, the total field at x_1 is calculated as the sum of the primary field which is the field free propagated in the half-space from x' to x_1, and the scattered field caused by the heterogeneities in the thin-slab between x' and x_1. The thickness of the slab should be made thin enough to ensure the validity of the local Born approximation. Under this condition, the Green's function can be approximated by the homogeneous half-space Green's function. The latter can be obtained by the image method (Morse and Feshbach, 1953). The stress should vanish at the free surface $z = 0$, leading to $\mu \partial u/\partial z = 0$, a Neumann boundary condition. Therefore, we have

$$g_0^h(\mathbf{r}_1; \mathbf{r}) = g_0(\mathbf{r}_1; \mathbf{r}) + g_0(\mathbf{r}_1; \mathbf{r}^*) \tag{12}$$

where g_0 is the infinite homogeneous Green's function and $\mathbf{r}^* = (x, -z)$ is the mirror image point of $\mathbf{r}$ with respect to the free surface.

Taking the Fourier transform of equation (11) along z_1, for the case of a thin-slab perpendicular to x-direction, we have

$$U(x_1, K_z) = k^2 \int_{x'}^{x_1} dx \int_0^\infty dz \{ g_0^h(x_1, K_z; x, z) \varepsilon_\rho(x, z) u_0(x, z) - \frac{1}{k^2} \nabla g_0^h(x_1, K_z; x, z) \cdot \varepsilon_\mu(x, z) \nabla u(x, z) \}. \tag{13}$$

We know the free space Green's function in wavenumber domain (Wu and Huang, 1995; Wu, 1996)

$$g_0(x_1, K_z; x, z) = \frac{i}{2\gamma} e^{i\gamma|x_1 - x|} e^{-iK_z z} \tag{14}$$

with

$$\gamma = \sqrt{k^2 - K_z^2}, \tag{15}$$

Therefore,

$$\begin{aligned} g_0^h(x_1, K_z; x, z) &= g_0(x_1, K_z; x, z) + g_0(x_1, K_z; x, -z) \\ &= \frac{i}{2\gamma} e^{i\gamma(x_1 - x)} [e^{-iK_z z} + e^{+iK_z z}] \\ &= \frac{i}{2\gamma} e^{i\gamma(x_1 - x)} 2 \cos(K_z z). \end{aligned} \tag{16}$$

In a similar way we can obtain

$$\nabla g_0(x_1, K_z; x, z) = \frac{1}{2\gamma}(\gamma\hat{e}_x + K_z\hat{e}_z)e^{i\gamma(x_1-x)}e^{-iK_z z} \quad (17)$$

and

$$\begin{aligned}\nabla g_0^h &= \frac{\partial}{\partial x} g_0^h\hat{e}_x + \frac{\partial}{\partial z} g_0^h\hat{e}_z \\ &= \frac{1}{2} e^{i\gamma(x_1-x)} \{\hat{e}_x 2\cos(K_z z) - \hat{e}_z(K_z/\gamma)2i\sin(K_z z)\}\end{aligned} \quad (18)$$

where $\hat{e}_x$ and $\hat{e}_z$ are unit vectors in the x and z directions, respectively.

Substitute g_0^h and ∇g_0^h into equation (13), leading to

$$\begin{aligned}U(x_1, K_z) &= U_\rho(x_1, K_z) + U_\mu(x_1, K_z) \\ U_\rho(x_1, K_z) &= \frac{ik}{2}\int_{x'}^{x_1} dx e^{i\gamma(x_1-x)} \\ &\qquad \int_0^\infty dz 2\cos(K_z z)\frac{k}{\gamma}\varepsilon_\rho(x, z)u_0(x, z) \\ U_\mu(x_1, K_z) &= -\frac{ik}{2}\int_{x'}^{x_1} dx e^{i\gamma(x_1-x)}\int_0^\infty dz[2\cos(K_z z)\bar{\partial}_x u_0 \\ &\qquad - 2i\sin(K_z z)\frac{K_z}{\gamma}\bar{\partial}_z u_0]\varepsilon_\mu(x, z)\end{aligned} \quad (19)$$

where

$$\begin{aligned}\bar{\partial}_x &= \frac{1}{ik}\frac{\partial}{\partial x} \\ \bar{\partial}_z &= \frac{1}{ik}\frac{\partial}{\partial z}\end{aligned} \quad (20)$$

are dimensionless partial derivatives. We can write these equations into

$$U_\rho(x_1, K_z) = \frac{ik}{2}\int_{x'}^{x_1} dx e^{i\gamma(x_1-x)} C\left[\frac{k}{\gamma}\varepsilon_\rho(z)u_0(z)\right] \quad (21)$$

$$\begin{aligned}U_\mu(x_1, K_z) &= -\frac{ik}{2}\int_{x'}^{x_1} dx e^{i\gamma(x_1-x)}\left\{C[\varepsilon_\mu(z)\bar{\partial}_x u_0(z)]\right. \\ &\qquad \left. - i\mathcal{S}\left[\frac{K_z}{\gamma}\varepsilon_\mu(z)\bar{\partial}_z u_0(z)\right]\right\}\end{aligned} \quad (22)$$

where $C[f(z)]$ and $\mathcal{S}[f(z)]$ are the cosine and sine transforms defined by

$$\begin{aligned}C[f(z)] &= \int_0^\infty dz 2\cos(K_z z)f(z) \\ \mathcal{S}[f(z)] &= \int_0^\infty dz 2\sin(K_z z)f(z)\end{aligned} \quad (23)$$

for forward transforms, and

$$\begin{aligned}C^{-1}[f(K_z)] &= \frac{1}{2\pi}\int_0^\infty dK_z 2\cos(K_z z)f(K_z) \\ \mathcal{S}^{-1}[f(K_z)] &= \frac{1}{2\pi}\int_0^\infty dK_z 2\sin(K_z z)f(K_z)\end{aligned} \quad (24)$$

for inverse transforms.

In equations (21) and (22) u_0, $\bar{\partial}_x u_0$ and $\bar{\partial}_z u_0$ can be calculated by

$$\begin{aligned}u_0(x, z) &= \frac{1}{2\pi}\int_{-\infty}^\infty dK_z' e^{iK_z' z}e^{i\gamma'(x-x')}u_0(x', K_z') \\ &= C^{-1}[e^{i\gamma'(x-x')}u_0(x', K_z')]\end{aligned} \quad (25)$$

and

$$\begin{aligned}\bar{\partial}_x u_0(x, z) &= C^{-1}[e^{i\gamma'(x-x')}\frac{\gamma'}{k}u_0(x', K_z')] \\ \bar{\partial}_z u_0(x, z) &= i\mathcal{S}^{-1}[e^{i\gamma'(x-x')}\frac{K_z'}{k}u_0(x', K_z')]\end{aligned} \quad (26)$$

Equations (21), (22), (25), and (26) are the dual-domain expressions of the wide-angle screen propagator for half-space *SH* problems.

Implementation Procedure for the Half-Space Wide-Angle Screen Propagator

Under the forward-scattering approximation we can update the total field with a marching algorithm in the forward direction. The half-space model can be sliced into thin-slabs perpendicular to the propagation direction. The weak scattering condition holds for each thin-slab. For each slab-step forward, the forward-scattered field from the thin-slab is calculated and added to the primary field so that the updated field becomes the incident field for the next thin-slab. The procedure can be summarized as follows:

1. Cosine transform the incident fields at the entrance of each thin-slab into wavenumber domain.
2. Free propagate in the wavenumber domain and calculate the primary field and its gradient within the slab.
3. At each horizontal position within the slab, inverse cosine/sine transform the primary field and its gradients into the space domain (25) and (26), and then interact with the medium perturbations ε_ρ and ε_μ.
4. Cosine/sine transform the distorted fields into the wavenumber domain and perform the divergence operations to get the scattered fields (21) and (22).
5. Calculate the primary field at the slab exit and add to the scattered field to form the total field as the incident field at the entrance of the next thin-slab.
6. Continue the procedure iteratively.

Small Angle Approximation and the Phase-Screen Propagator

When the energy of crustal guided waves is carried mainly by small-angle waves (with respect to the horizontal direction), the small angle approximations can be invoked to simplify the theory and calculations. Let us first consider the calculations for U_μ. Substitute (26) into (22), resulting in

$$U_\mu(x_1, K_z) = -\frac{ik}{2}\int_{x'}^{x_1} dx e^{i\gamma(x_1-x)}\frac{1}{2\pi}\int_0^\infty dK_z' e^{i\gamma'(x-x')}\int_0^\infty dz \left\{2\cos(K_z z)\varepsilon_\mu(z) 2\cos(K_z' z)\left(\frac{\gamma'}{k}\right) + 2\sin(K_z z)\varepsilon_\mu(z) 2\sin(K_z' z)\left(\frac{K_z}{\gamma}\right)\left(\frac{K_z'}{k}\right)\right\} u_0(x', K_z') \quad (27)$$

This is the local Born scattering in wavenumber domain. Equation 27 can be written as

$$U_\mu(x_1, K_z) = \mathbf{A}_\mu u_0(x', K_z') \quad (28)$$

where $\mathbf{A}_\mu$ is an operator. In the discrete form, it is a matrix, whose elements are incident and outgoing (scattered) wavenumbers dependent. For small-angle waves, $K_z \ll \gamma \approx \gamma' \approx k$. The second term of equation (27) is a second-order small quantity compared with the first term, and therefore can be neglected in this case. Then we have

$$U(x_1, K_z) = U_\rho(x_1, K_z) + U_\mu(x_1, K_z) = -\frac{ik}{2} e^{i\gamma(x_1-x')} \frac{1}{2\pi}\int_0^\infty dK_z' 2\cos(K_z' z)\int_0^\infty dz 2\cos(K_z z) \int_{x'}^{x_1} dx e^{i(\gamma-\gamma')(x-x')}\left[\left(\frac{k}{\gamma}\right)\varepsilon_\rho(z) - \left(\frac{\gamma'}{k}\right)\varepsilon_\mu(z)\right] u_0(x', K_z') \approx ike^{i\gamma(x_1-x')} C[S_s(z) u_0(x', z)] \quad (29)$$

where

$$S_s(z) = \frac{1}{2}\int_{x'}^{x_1} dx[\varepsilon_\rho(x, z) - \varepsilon_\mu(x, z)] \approx \Delta x \bar{\varepsilon}_s(z) \quad (30)$$

where $\bar{\varepsilon}_s(z)$ is the average *S*-wave slowness perturbation over the thin-slab at depth z, $\bar{\varepsilon}_s(z) = 1/(x_1 - x')\int_{x'}^{x_1} dx(s(x) - s_0)/s_0$ with $s(x) = 1/v(x)$, $\Delta x = (x_1 - x')$ is the thin-slab thickness. Here S_s is the corresponding slowness screen for the half-space thin-slab. Equation (29) is the screen approximation of the half-space *SH* problem. Summing up the primary and scattered fields and invoking the Rytov transform result in the dual-domain expression of phase-screen propagator for this case

$$u(x_1, K_z) = u_0(x_1, K_z) + U(x_1, K_z) = e^{i\gamma(x_1-x')}\int_0^\infty dz 2\cos(K_z z)[1 + ikS_s(z)]u_0(x', z) \approx e^{i\gamma(x_1-x')} C[e^{ikS_s(z)} u_0(x', z)] \quad (31)$$

where $e^{ikS_s(z)}$ is the phase delay operator.

Implementation Procedure for the Half-Space Phase-Screen Propagator

Under the phase-screen approximation, the heterogeneous half-space is represented by a series of half-screens embedded in the homogeneous background half-space. The wave propagates between screens in the wavenumber domain and interacts with the phase-screens in the space domain. The interaction is only a phase-delay operator (multiplication in space domain). The procedure can be summarized as follows:

1. Cosine transform the incident field at the starting plane into wavenumber domain and free propagate to the screen.
2. Inverse cosine transform the incident field into space domain and interact with the shear slowness screen (phase-screen) to get the transmitted field.
3. Cosine transform the transmitted field into wavenumber domain and free propagate to the next screen.
4. Repeat the propagation and interaction screen-by-screen to the boundary of the model space.

Treatment of the Moho discontinuity

The Moho discontinuity can be treated in two ways. One is to put the impedance boundary conditions in the formulation, the other is to treat the parameter changes as perturbations and therefore be incorporated into the screen interaction. The former has the advantage of computational efficiency. The latter has the flexibility of handling irregular interfaces. In this article, we adopt the latter approach and check the validity of perturbation approach for the Moho discontinuity by theoretical analysis and numerical comparison with other methods.

To simplify the analysis, we consider here only the flat Moho reflections without the free surface. In this case, a whole space Green's function with the crust velocity as reference velocity is used and the scattered field in the wavenumber domain under the small-angle approximation can be written as

$$U(x_1, K_z) = i\omega(s_2 - s_1)\Delta x e^{i\gamma(x_1-x)}\int_{z_M}^\infty dz e^{-iK_z z} u_0(x, z) \quad (32)$$

where z_M is the depth of Moho, and $s_1 = 1/\beta_1$, $s_2 = 1/\beta_2$ are the crust and mantle slownesses, respectively. Since slowness perturbations exist only below the Moho ($z > z_M$), the integration starts from z_M. The reflected crust wave is formed by the scattered field with negative K_z (upgoing).

Given this flat Moho with two homogeneous half-spaces, the crustal (reflected) wave does not affect the mantle wave, whereas the mantle wave will influence the upgoing crustal wave through updating the incident field in the mantle. In this way the mantle wave, which is mainly inhomogeneous wave such as head wave in the case of critical and postcritical reflections, can be calculated by an independent equation. In space domain, it can be written as

$$U^M(x_1, z_1) = i\omega\Delta x(s_2 - s_1)\frac{1}{2\pi}\int_{-\infty}^{\infty} dK_z \int_{z_M}^{\infty} dz e^{i\gamma\Delta x + iK_z(z_1 - z)} u_0(x, z) = i\omega\Delta x(s_2 - s_1) A_S u_0(x, z) \quad (33)$$

where A_S is a symbolic expression of the scattering operator. Note that the incident wave u_0 is the wave field output from the previous step and propagate one step Δx forward using the background velocity, the crustal velocity. In fact, after the phase correction $\omega\Delta x(s_2 - s_1)$, the mantle wave propagating along the horizontal direction will have the exact propagation speed. This implicates the precise propagation for head waves. For each step Δx, the incident wave in the mantle is updated. For the case of wide-angle generalized screen approximation, a similar expression can be obtained with a more complicated scattering operator A_S, which improves the accuracy of large-angle mantle waves.

The generalized screen formulation, especially the phase-screen approximation, is accurate for small-angle propagating waves with respect to the horizontal direction in this geometry. We know that for guided waves, or crustal waves near critical angles, the related mantle waves are nearly horizontal. Therefore, the screen approximation is quite accurate in this case. A formal accuracy analysis for the phase-screen approximation has been performed by Huang and Fehler (1998), and a more general accuracy analysis for various generalized screen approximations can be found in de Hoop *et al.* (1999).

For a standard crustal waveguide with $V_{\text{crust}} = 3.5$ km/sec and $V_{\text{mantle}} = 4.5$ km/sec, the critical angle for crustal waves is 51°, which corresponds to an incident angle 39° (with respect to the x-direction) for our screen method. The relative velocity perturbation is 29%. This leads to a relative phase error of 6% based on Huang and Fehler (1998) equation (47) for the inaccurate expression of the square-root operator of wave equation. This phase error will be translated into a small error in refraction angle. However, as we already mentioned, the propagation process in the screen method is an updating process in the x-direction. At each subsequent step, the propagation angle below the Moho is gradually corrected to nearly horizontal for critical or postcritical crust waves. Therefore the reflection and refraction are exact for crustal waves at or beyond the critical angle. The effect of the small phase error of the screen approximation is to broaden the transition zone from precritical to critical reflections and introduce amplitude errors in precritical reflections. At and beyond the critical angle, the propagation is exact for both the crustal waves and mantle waves (head waves).

Figure 1 shows the comparison between the theoretical reflection coefficients (dotted line) and the calculated ones by the phase-screen method (solid line) for a standard Moho ($V_c = 3.5$ km/sec, $g_c = 2.8$ g/cm^3, $V_m = 4.5$ km/sec, $g_m = 3.1$ g/cm^3). The curve from the screen method is obtained by using the RMS of the reflected waveforms. We see that the process of critical reflection is well matched, except the transition from precritical to critical calculated by the screen method is not as sharp as the theoretical curve. This may be caused by the small phase error in the phase-screen approximation. In addition, the reflections for small-angle incidence, especially for nearly vertical incidence, are not well modeled by the phase-screen method. The wide-angle formulation can improve the small-angle response to some degree, but the accuracy for this case will be still limited. However, this limitation is only for short distance propagations, well before the critical distance, around 80 km in the case of standard crust model. The screen method behaves very well beyond the critical distance, making it a good candidate for guided wave simulations. Figure 2 shows the comparison of Moho reflections calculated by a finite-difference method (thin line) and by the screen method (thick line). We see that beyond 55 km, the two curves agree quite well. The top panel of Figure 3 is a standard crust model. The bottom panel is the energy attenuation versus distance. We see that beyond the critical distance, the guided waves are formed and all the wave energy is trapped in the crustal waveguide. This further approves the validity of the generalized screen approach for modeling crustal guided waves. The middle panel shows the angular spectral variation along the propagation path. In the

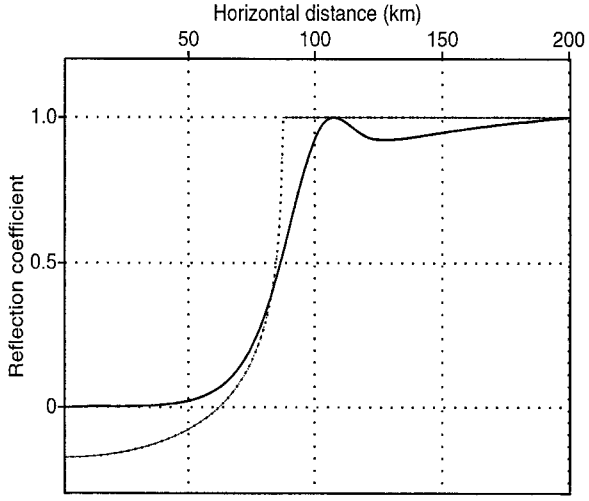

Figure 1. Comparison of reflection coefficients between theoretical (dotted line) and the calculated one by screen method (solid line).

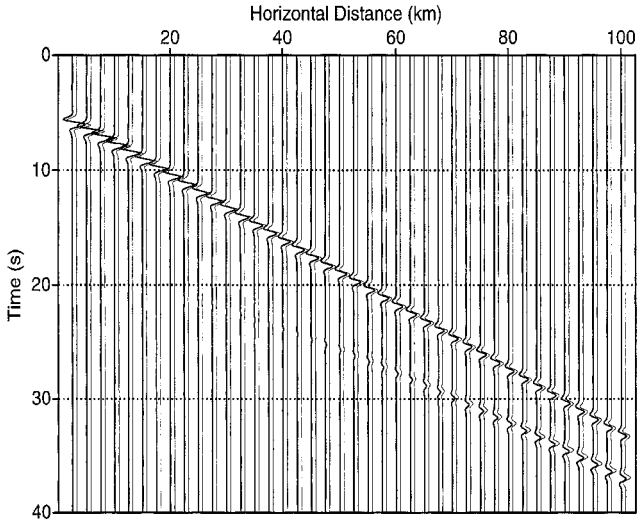

Figure 2. Comparison of synthetic seismograms between the screen method and the fourth-order finite difference method for Moho reflection without free surface. The source function is a Gaussian derivative. The first and second arrivals are the direct and reflected waves, respectively.

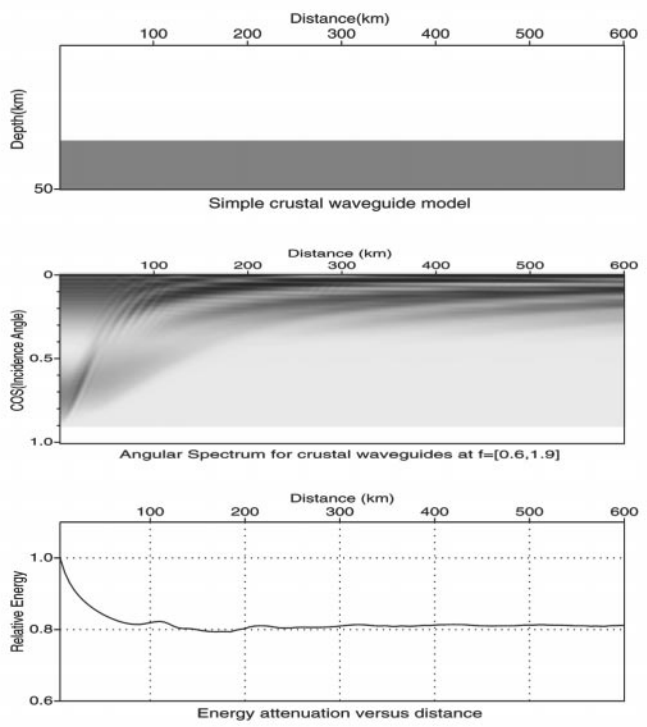

Figure 3. Energy variation and angular spectrum versus distance for flat crustal waveguide model. The top panel is the flat crust model in which the parameters of velocity and density are 3.5 km/sec and 2.8 g/cm^3 in crust, 4.5 km/sec and 3.3 g/cm^3 in mantle, respectively. The middle panel is the angular spectrum versus distance, which shows the guided energy trapped in the crust at and beyond the critical angle. The bottom panel shows the relative energy distribution along the path.

beginning, the angular spectra are broad and the energy leakage is strong. Beyond the critical angle, small wavenumber (small angle to the horizontal axis) waves become dominant and guided modes are formed. In summary, from the comparison of reflection coefficients at and beyond the critical angle, from the trapped energy of guided waves and mode formation, the validity of the screen approximation in treating the Moho reflections for guided waves can be approved.

Wide-Angle Screen Propagator and Phase-Screen Propagator

From earlier derivations we know that the wide-angle propagator should be more accurate than the phase-screen propagator. Accuracy analysis and numerical tests for different screen approximations can be found in Wu and de Hoop (1996), Huang and Wu (1996), and de Hoop *et al.* (1999). If we take the wave velocity in the crust as the reference velocity for the screen propagator, the differences between the seismograms calculated by these two screen propagators are unnoticeable for large-angle waves (with respect to the vertical axis). However, when velocity variation in the crust is large, the difference between these two approximations becomes more significant. For sake of simplicity, we test the accuracy of wide-angle screen and phase-screen propagators for a model of two half-spaces (crust and mantle) without the free surface. Figure 4 shows the comparison of seismograms calculated by the two approximations when the reference medium for the propagators is set to be much different from the crust (v_0 = 2.9 km/sec, ρ_0 = 2.7 g/cm^3; i.e., the crust has 21% and the mantle has 55% velocity perturbations from the reference medium). The thick lines are from the wide-angle screen and the thin lines are from the phase-screen. We can clearly see the difference in both amplitude and arrival time of the reflected waves when the reflection angles are small (small epicenter distances).

In normal situations, the reference medium can be chosen as the same as the local crust, and vary along the horizontal direction. For crustal heterogeneities, such as small-scale random perturbations, the velocity contrasts are usually less than 10%. Therefore we can safely apply the phase-screen propagator in most cases. For this reason, in all the following examples the phase-screen propagator is adopted.

Numerical Verification and Tests

To test the validity of the half-space GSP method (or simply call it the screen method), we have conducted extensive numerical tests and checked the results with various well-known numerical methods, such as the wavenumber integration and finite difference methods.

First, in Figure 5 we show the accuracy of the method by comparing the synthetic seismograms generated by the screen method (thick lines) with those calculated by a re-

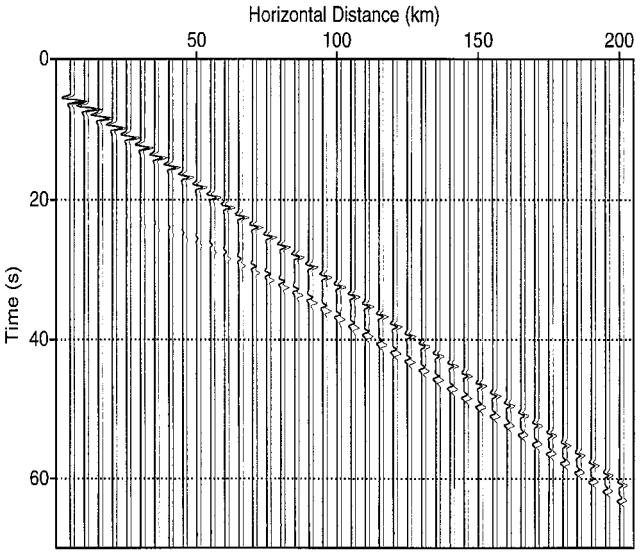

Figure 4. Comparison of reflection seismograms using small- and wide-angle screen propagators. The reference velocity and density used in calculation are 2.9 km/sec and 2.7 g/cm^3. The parameters of the crust and the mantle are the same as the previous examples.

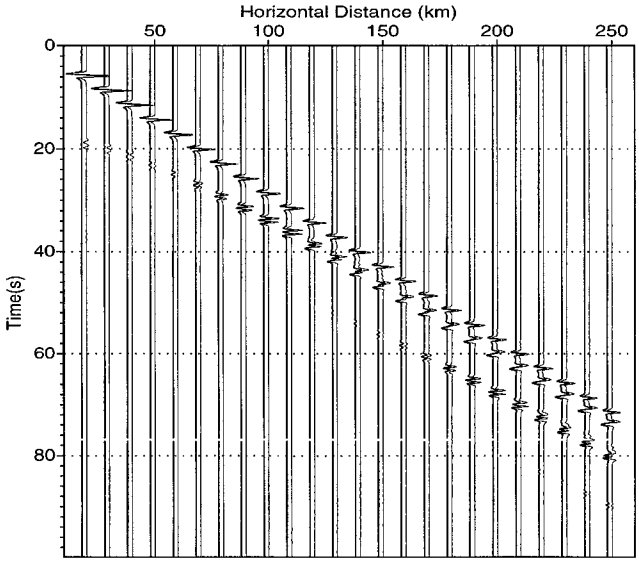

Figure 5. Comparison of synthetic seismograms along the surface calculated by the screen method (thick lines) and reflectivity method (thin lines) for a flat crustal model (32 km thick). The source function is a Ricker wavelet with dominant frequency of 1.0 Hz.

flectivity method (thin lines) for a uniform crustal model. The crust has a thickness of 32 km and a shear wave velocity of 3.5 km/sec. The mantle beneath the crust has a shear velocity of 4.5 km/sec. The source depth is 2 km and the source time function is a Ricker wavelet with a dominant frequency of 1.0 Hz. Our results agree very well with the reflectivity method, which is considered very accurate for flat layered media. The only exceptions are for near vertical reflections at very small epicentral distances where the screen method has low accuracy for extremely large scattering angles with respect to the propagation direction. However, since regional seismograms are usually recorded at large distances, this limitation does not pose any real problem for its application. Next, we show the accuracy of the method by comparing synthetic seismograms generated by this method with those generated by a finite difference algorithm (Xie and Lay, 1994). For the finite difference method, a fourth-order elastic *SH*-wave code is used to calculate the synthetic seismograms. The spatial sampling interval is 0.125 km in both vertical and horizontal directions, and the time interval is 0.015 sec. For the screen method, the spatial sampling interval is 0.25 km in the vertical direction and the screen interval is 1.0 km. For both methods the source depth is 2 km and the source time function is a Gaussian derivative. Because of the computational intensity of the finite difference method, we did the comparison at short propagation distances (250 km) and a relatively low frequency ($f_0 \sim 0.5$ Hz). Figure 6 gives the comparison between synthetic seismograms from the screen method and from the finite difference method for the same flat layered model. Their agreement is excellent.

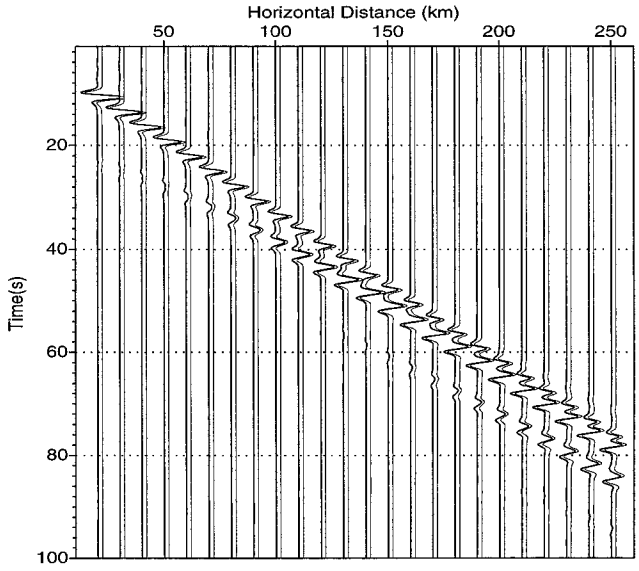

Figure 6. Comparison of synthetic seismograms along the surface calculated by the screen method (thick lines) and the fourth-order finite difference method (thin lines) for a flat crustal model (32 km thick). The source function is a Gaussian derivative ($f_0 \sim 0.5$ Hz).

Next we show the comparison for a heterogeneous crustal model. On the top of Figure 7 is the crust model with a narrow passage ("neck" type) used to calculate synthetic seismograms. On the bottom are the synthetic seismograms along a vertical profile at an epicentral distance of 250 km.

The thin lines are from the finite difference method and the thick lines are from the screen method. The source is located at a depth of 2 km and the source time function has a dominant frequency of 0.5 Hz. Excellent agreement can be seen. For this example, the GSP method took 20 CPU minutes on a SPARC-4. To obtain a similar accuracy, the FD calculation (a *SH* version of Xie and Lay, 1994) took 3000 CPU minutes on a SPARC-20. The speed factor is about 300.

We have performed an accuracy comparison between the screen method and finite difference method for different grid spacings. It was found that when the grid spacing for the finite difference method is 0.25 km, which still satisfies the stability criterion, there are considerable discrepancies between the results of the two methods (see the figure in Wu *et al.*, 1997). This is due to the numerical dispersion of the finite difference method. With a finer grid spacing of 0.125 km, the results from finite difference converged to those of the GSP method. This shows that for wave propagation in the crustal waveguide, the finite difference method requires a finer grid than that required by conventional stability criterion. The grid spacing (Δz) of the screen method for the comparison is 0.5 km, and the screen interval (Δx) is 1 km.

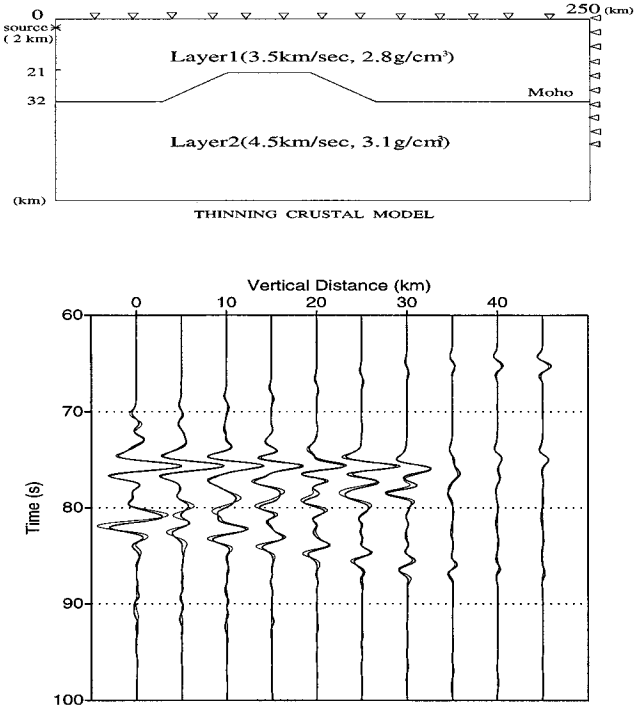

Figure 7. Comparison of synthetic seismograms along a vertical profile at the distance of 250 km calculated by the screen method (thick lines) and a finite difference method (thin lines) for a laterally varying crustal model shown on the top panel.

Examples of Lg Propagation Using the Screen Method

In this section we show some examples demonstrating the potential of the method applied to various problems of regional wave propagation.

Long Range Lg Propagation Simulation in Complex Crustal Waveguides

Visualize the Path Effects by Snap Shots. The high efficiency of the method permits the simulation of high-frequency Lg wave propagation through long crustal wave guides. The snap shots can be easily generated to visually analyze the path effects of Lg wave propagation. Figures 8 to 10 show the snap shots calculated by the screen method for waveguides at 30, 50, and 70 sec, respectively. In each figure, from top to bottom are results for flat, narrowing, and broadening crustal waveguides respectively. The source is located on the left boundary at a depth of 2 km. The development of mantle wave and head wave, as well as the formation of crustal guided waves as multiple reflections between free surface and Moho discontinuity can be clearly seen. For the inhomogeneous models, wave diffraction, leakage to the mantle, wavefront distortion, and increase of wave field complexity can also be seen clearly. From the comparison it is seen that the passage of a narrow crustal waveguide ("neck" type) has greater effect on Lg leakage than the broad passage ("belly" type). In the latter case, although the wavefronts are complicated due to scattering at the edges, there is more energy trapped in the crust than the case of narrow passage in which a large percentage of energy leaks into the mantle. This example demonstrates the potential of the method as a tool for investigating the path effects of different crustal structures.

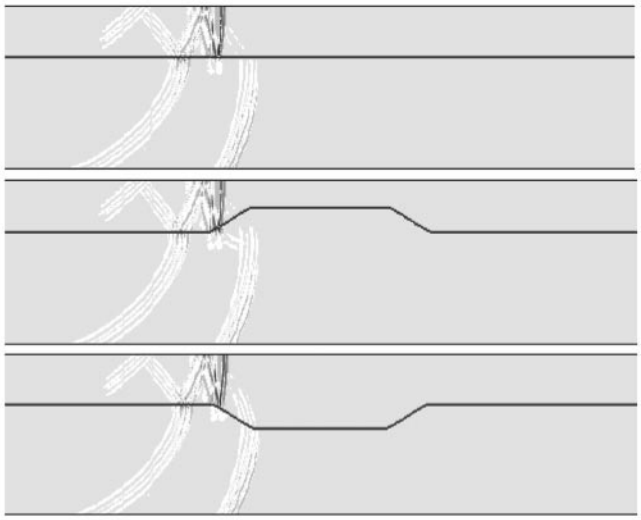

Figure 8. Snap shots at 30 sec. The development of mantle waves and head waves can be seen clearly.

Long-Range High-Frequency Synthetic Seismograms. The following example shows the capability of this method for long-range high-frequency synthetic seismograms in a lat-

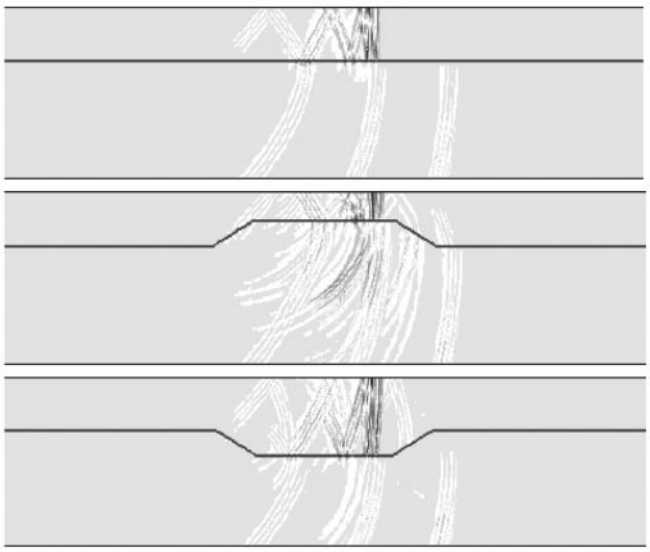

Figure 9. Snap shots at 50 sec. The development of mantle waves and head waves, and the influence of crust thining and thickening, can be seen clearly.

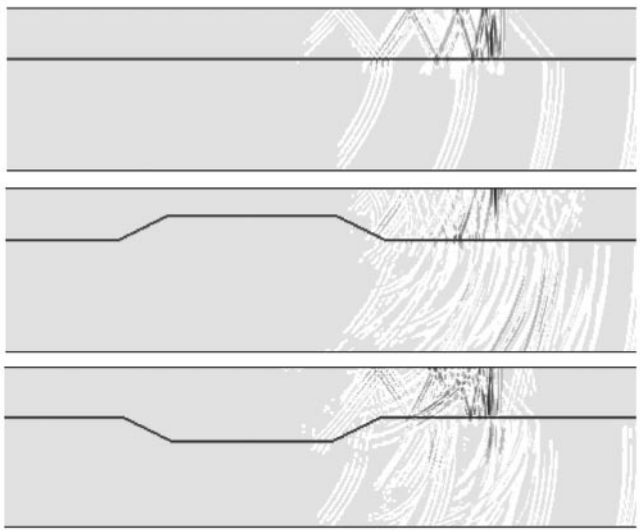

Figure 10. Snap shots at 70 sec. The development of mantle waves and head waves, and the influence of crust thining and thickening, can be seen clearly.

erally varying structure. Figure 11 shows the laterally varying crust model used in the calculation. Figure 12 shows the high-frequency synthetic seismograms on the surface at distances up to 1000 km for the model. The center frequency is 5 Hz with the maximum frequency of 10 Hz. The low-frequency (f_c = 1 Hz, f_{max} = 2 Hz) synthetic seismograms are shown in Figure 13. As can be seen, the effect of the waveguide narrowing is different for low and high frequencies. It is also clear that without high-frequency content, many of the distinctive features associated with Lg measurements cannot be adequately modeled. In other words, a proper simulation method with the capability to generate ac-

Parameters of Crustal Model

Layer	Vs(km/sec)	Density(g/cm^3)	Thickness(km)
1	3.00	2.60	1.00
2	3.70	3.00	31.00
3	4.50	3.30	Half-Space

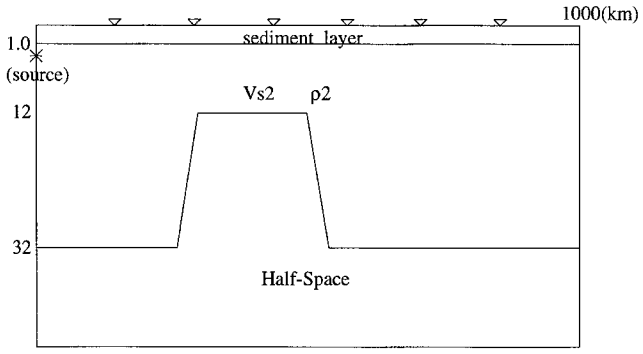

Crustal Model

Figure 11. An inhomogeneous crustal model used in the calculation of high-frequency synthetic seismograms. Shown in the upper panel are model parameters and the lower panel gives the geometry of the model. The receivers are on the surface and shown by triangles.

curate high-frequency signals is necessary to investigate regional phases.

The Influences of Random Heterogeneities

The importance of small-scale random heterogeneities to seismic wave propagation is well known. There are extensive publications on this subject in seismology. However, the role of random heterogeneities in Lg excitation, propagation, attenuation, and blockage is still unclear due to the complexity of the problem. The theory of wave propagation in unbounded random media has been well developed. However, for waves in complex crustal waveguides with random heterogeneities, the theoretical difficulties are overwhelming, and no analytical tools are available for performing realistic calculations. Numerical simulation is an attractive alternative to the theory. Some finite difference simulations have been conducted (e.g., Frankel and Clayton, 1986; Frankel, 1989; Xie and Lay, 1994; Jih, 1996). Limited by the computation power, however, the propagation distances of the finite difference simulations are relatively short. Liu and Wu (1994) have done some numerical simulation using the phase-screen method, but the media simulated are limited to unbounded media. The development of the half-space GSP method enables us to simulate high-frequency waves propagating in complex crustal waveguides to long distances. In the following section, we will show two examples demonstrating the capability of the method.

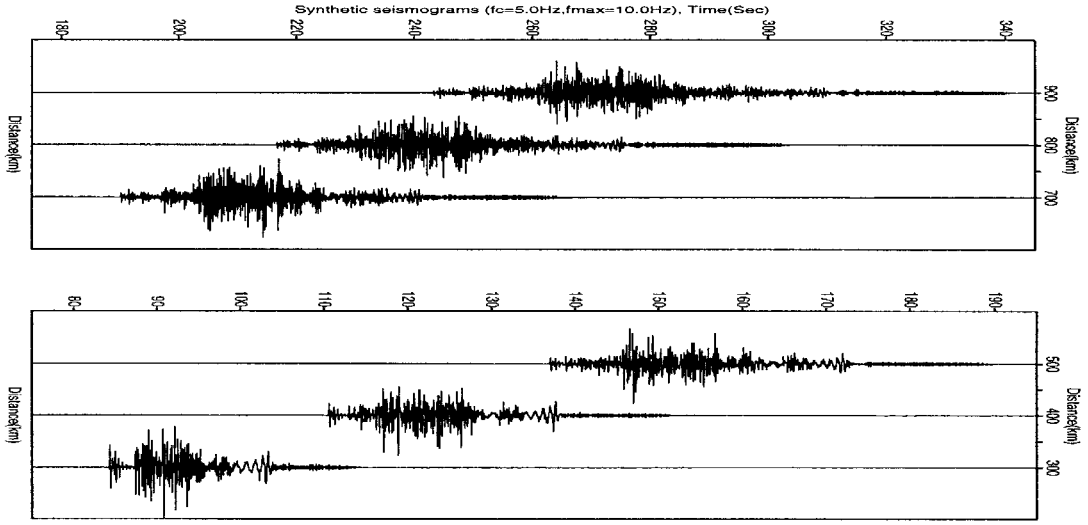

Figure 12. High-frequency (f_c = 5 Hz, f_{max} = 10 Hz) synthetic seismograms on the surface at distances up to 1000 km for an inhomogeneous crustal waveguide.

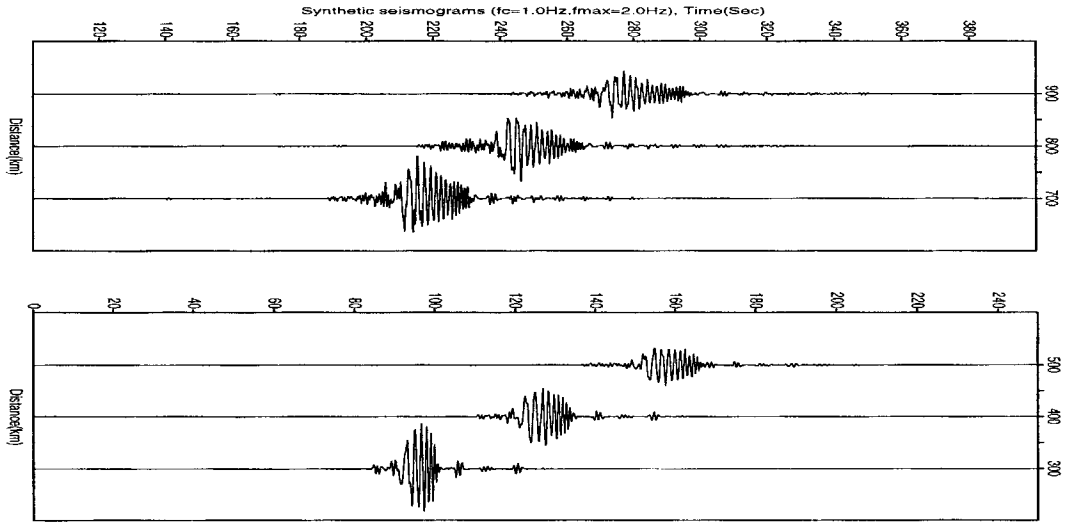

Figure 13. Low-frequency (f_c = 1 Hz, f_{max} = 2 Hz) synthetic seismograms on the surface at distances up to 1000 km for an inhomogeneous crustal waveguide.

Figure 14 shows a heterogeneous crustal model representing a "mountain root" with small-scale random heterogeneities. On the top panel is the velocity model, and the comparisons between synthetic seismograms with and without random heterogeneities are shown on the middle and bottom panels, respectively. The heterogeneities have an exponential correlation function, with the scale length $a_x = a_z$ = 1.6 km (in horizontal and vertical directions, respectively). The RMS velocity perturbation is 5%. The dominant frequency of the source function is 2 Hz. Figures 15a and 15b show the comparison between snap shots for waves passing through the "mountain root" with and without random heterogeneities, respectively. We see that random heterogeneities drastically increase the leakage of waves to the mantle and the complexity of the waveforms. Extensive numerical experiments will be conducted to study the different influences of various kinds of random heterogeneities. It has been shown that the crustal random heterogeneities are highly anisotropic in scale length (Levander and Holliger, 1992; Holliger and Levander, 1992; Wu *et al.*, 1994). The influences of the random heterogeneities with different stochastic characteristics will be explored systematically.

Conclusion

The advantages of the half-space GSP method can be summarized as follows.

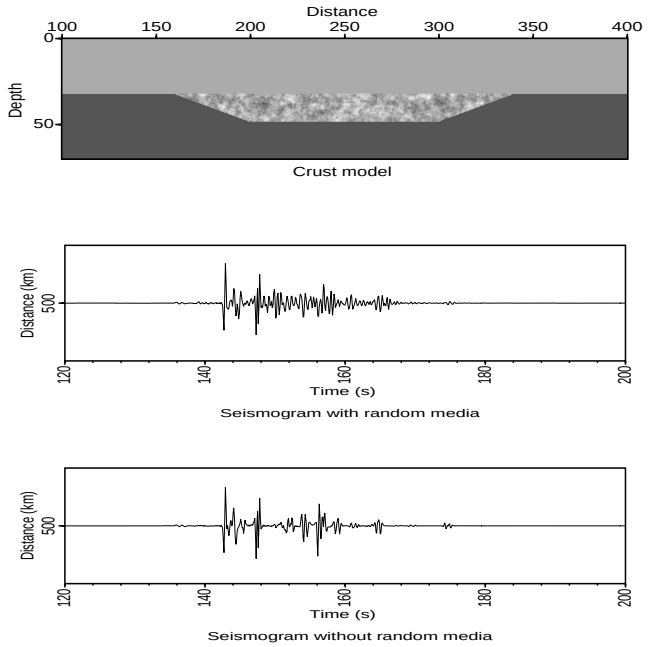

Figure 14. A heterogeneous crustal model representing a mountain root with small-scale random heterogeneities (top panel). The comparison between synthetic seismograms with and without random heterogeneities are shown on the middle and bottom panels, respectively.

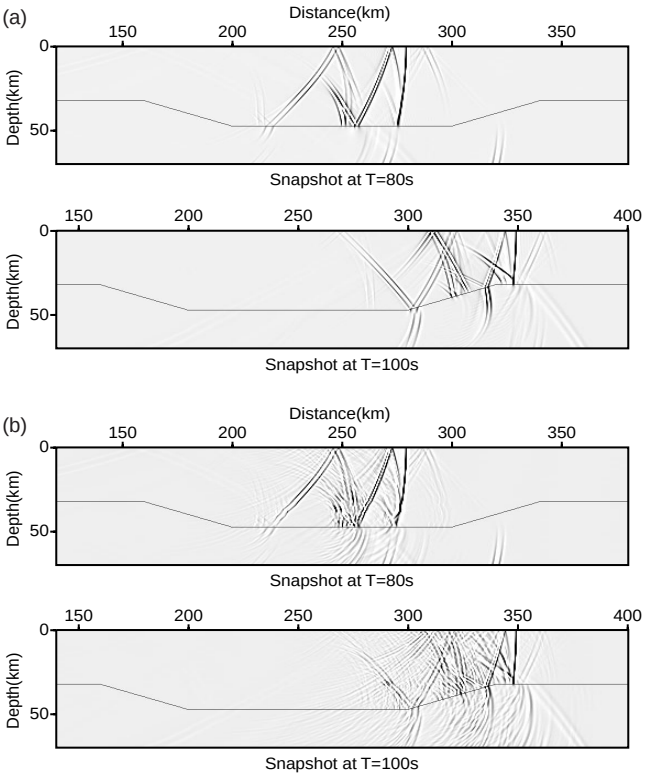

Figure 15. Comparison between snapshots for waves passing through a 'mountain root' (a) with or (b) without random heterogeneities.

- Fast speed: For medium size 2D Lg problems, it is 2–3 orders of magnitude faster than the finite difference methods. For large distance, high frequency 3D problems, the time saving factor could be much greater.
- Memory saving: The GSP needs only to store 2D data arrays for each step instead of 3D volume data, leading to huge memory savings. For the *SH* problems in this article, GSP needs only to store 1D data arrays.
- Stability: The transversal Laplacian is calculated by the Fourier method; therefore, no numerical dispersion occurs for high frequency waves.
- Intrinsic attenuation: Being a frequency domain method, it is easy to incorporate various Q models into the simulation. Therefore, the method can study the effects of scattering and anelasticity on Lg wave blockage and attenuation.
- Random heterogeneities: Random heterogeneities can also be easily incorporated into the model. The effects of small-scale heterogeneities and their statistical characteristics can be studied by numerical simulations using this method.

The use of a half-space phase-screen propagator has made the seismogram synthesis in the regional distances very efficient. The rapid change of crustal structures and small-scale heterogeneities in the crust can be easily handled. The results in this article demonstrates the advantages and feasibility of the approach. *P-SV* and full 3D problems will be treated in future publications.

The fundamental assumption of the screen propagators is the one-way propagation, which neglects backscattering. However, as demonstrated by previous studies (e.g., Cao and Muirhead, 1993; Bouchon and Coutant, 1994), backscattering from structural barriers also contributes to the Lg energy loss. Therefore, when strong backscattering is expected for a certain path, attention should be paid to the limitation of GSP simulations.

Acknowledgments

The helpful discussions with T. Lay, L. J. Huang, and X. F. Chen are appreciated. The paper has benefitted from the comments and suggestions of M. Bouchon, B. L. N. Kennett, T. Furumura, and R. Gibson. The work was supported by the Air Force Office of Scientific Research through Contract F49620-95-1-0028 and by the Department of Energy through Contract F19628-95-K-0016, administered by the Phillips Laboratory of the Air Force. The facility support from the W. M. Keck Foundation is also acknowledged. Contribution number 341 of the Institute of Tectonics, University of California, Santa Cruz.

References

Aki, K., and P. G. Richards (1980). *Quantitative Seismology: Theory and Methods*, Vol. 1 and 2, W.H. Freeman, New York.

Bostock, M. G., and B. L. N. Kennett (1990). The effect of 3-D structure on Lg propagation patterns, *Geophys. J. Int.* **101,** 355–365.

Bouchon, M., and O. Coutant (1994). Calculation of synthetic seismograms in a laterally varying medium by the boundary element-discrete wavenumber method, *Bull. Seism. Soc. Am.* **84,** 1869–1881.

Campillo, M. (1990). Propagation and attenuation characteristics of the crustal phase Lg, *Pure Appl. Geophys.* **132,** 1–19.

Campillo, M., and A. Paul (1992). Influence of lower crustal structure on the early coda of regional seismograms, *J. Geophys. Res.* **97,** 3405–3416.

Campillo, M., B. Feignier, M. Bouchon, and N. Bethoux (1993). Attenuation of crustal waves across the Alpine range, *J. Geophys. Res.* **98,** 1987–1996.

Cao, S., and K. Muirhead (1993). Finite difference modeling of Lg blockage, *Geophys. J. Int.* **115,** 85–96.

de Hoop, M. V., R. S. Wu, and J. le Rousseau (1999). General formulation of screen methods for the scattering of waves in inhomogeneous media, *Wave Motion* (in press).

de Wolf, D. A. (1971). Electromagnetic reflection from an extended turbulent medium: cumulative forward-scatter single-backscatter approximation, *IEEE Trans. Ant. Propag.* **AP-19,** 254–262.

de Wolf, D. A. (1985). Renormalization of EM fields in application to large-angle scattering from randomly continuous media and sparse particle distributions, *IEEE Trans. Ant. Propag.* **AP-33,** 608–615.

Frankel, A. (1989). A review of numerical experiments on seismic wave scattering, in *Scattering and Attenuation of Seismic Waves, II*, R. S. Wu and K. Aki (Editors), Birkhauser, Berlin, 639–686.

Frankel, A., and R. W. Clayton (1986). Finite difference simulations of seismic scattering: implications for propagation of short-period seismic waves in the crust and models of crustal heterogeneity, *J. Geophys. Res.* **91,** 6465–6489.

Furumura, T., and B. L. N. Kennett (1997). On the nature of regional seismic phases—II. On the influence of structural barriers, *Geophys. J. Int.* **129,** 221–234.

Gibson, R. L., and M. Campillo (1994). Numerical simulation of high- and low-frequency Lg-wave propagation, *Geophys. J. Int.* **118,** 47–56.

Goldstein, P., C. Schultz, S. Larsen, and L. Minner (1996). Modeling of regional wave propagation phenomena in the middle east and north Africa and new analysis capabilities in SAC2000, in *Proceedings of the 18th Annual Seismic Research Symposium on Monitoring a Comprehensive Test Ban Treaty*, J. F. Lewkowicz, J. M. McPhetres, and D. T. Reiter (Editors), 165–171.

Holliger, K., and A. R. Levander (1992). A stochastic view of lower crustal fabric based on evidence from the Ivrea zone, *Geophys. Res. Lett.* **19,** 1153–1156.

Huang, L. J., and M. C. Fehler (1998). Accuracy analysis of the split-step fourier propagator: implications for seismic modeling and migration, *Bull. Seism. Soc. Am.* **88,** 18–29.

Huang, L. J., and M. C. Fehler, and R. S. Wu (1999a). Extended local Born Fourier migration method, *Geophysics* **64,** 1524–1534.

Huang, L. J., M. C. Fehler, P. M. Roberts, and C. C. Burch (1999b). Extended local Rytov Fourier migration method, *Geophysics* **64,** 1535–1545.

Huang, L. J., and R. S. Wu (1996). 3D prestack depth migration with acoustic pseudo-screen propagators, *Mathematical Methods in Geophysical Imaging IV, SPIE* **2822,** 40–51.

Jih, R. S. (1996). Waveguide effects of large-scale structural variation, anelastic attenuation, and random heterogeneity on SV Lg propagation: a finite-difference modeling study, in *Proceedings of the 18th Annual Seismic Research Symposium on Monitoring a Comprehensive Test Ban Treaty*, J. F. Lewkowicz, J. M. McPhetres, and D. T. Reiter (Editors), 182–194.

Kennett, B. L. N. (1984). Guided wave propagation in laterally varying media—I. Theoretical development, *Geophys. J. R. Astr. Soc.* **79,** 235–255.

Kennett, B. L. N. (1986). Lg waves and structural boundaries, *Bull. Seism. Soc. Am.* **76,** 1133–1141.

Kennett, B. L. N. (1989). Lg-wave propagation in heterogeneous media, *Bull. Seism. Soc. Am.* **79,** 860–872.

Kennett, B. L. N. (1990). Guided wave attenuation in laterally varying media, *Geophys. J. Int.* **100,** 415–422.

Kennett, B. L. N. (1998). Guided waves in three-dimensional structures. *Geophys. J. Int.* **133,** 159–174.

Kennett, B. L. N., M. G. Bostock, and J. K. Xie (1990). Guided-wave tracking in 3-D—A tool for interpreting complex regional seismograms *Bull. Seism. Soc. Am.* **80,** 633–642.

Kosloff, D., D. Kessler, A. Quieroz, and E. Tessmer (1990). Solution of the equations of dynamic elasticity by a Chebychev spectral method, *Geophysics* **55,** 734–748.

Levander, A., and K. Holliger (1992). Small-scale heterogeneity and large-scale velocity structure of the continental crust, *J. Geophys. Res.* **97,** 7897–8804.

Liu, Y. B., and R. S. Wu (1994). A comparison between phase-screen, finite difference and eigenfunction expansion calculations for scalar waves in inhomogeneous media, *Bull. Seism. Soc. Am.* **84,** 1154–1168.

Maupin, V. (1989). Numerical modeling of Lg wave propagation across the North Sea central graben, *Geophys. J. Int.* **99,** 273–283.

Maupin, V., and B. L. N. Kennett (1987). On the use of truncated model expansion in laterally varying media, *Geophys. J. R. Astr. Soc.* **91,** 837–851.

Morse, P. M., and H. Feshbach (1953). *Methods of Theoretical Physics*, McGraw-Hill, New York, 812–813.

Orrey, J., C. Archambeau, and G. Frazier (1996). Complete seismic wave field synthesis with a pseudospectral method: the generalized Fourier method, *Geophys. J. Int.* (submitted for publication).

Schatzman, J. C. (1996). A pseudo-spectral scheme for viscoelastic seismic modeling, *Proceedings of the 18th Annual Seismic Research Symposium on Monitoring a Comprehensive Test Ban Treaty*, J. F. Lewkowicz, J. M. McPhetres, and D. T. Reiter (Editors), 261–270.

Wild, A. J., and J. A. Hudson (1997). A geometrical approach to the elastic complex screen, *J. Geophys. Res.* **103,** 707–725.

Wu, R. S. (1994). Wide-angle elastic wave one-way propagation in heterogeneous media and an elastic wave complex-screen method, *J. Geophys. Res.* **99,** 751–766.

Wu, R. S. (1996). Synthetic seismograms in heterogeneous media by one-return approximation, *Pure Appl. Geophys.* **148,** 155–173.

Wu, R. S., and M. V. de Hoop (1996). Accuracy analysis and numerical tests of screen propagators for wave extrapolation, *Mathematical Methods in Geophysical Imaging IV, SPIE* **2822,** 196–209.

Wu, R. S., and L. J. Huang (1995). Reflected wave modeling in heterogeneous acoustic media using the de Wolf approximation, *Mathematical Methods in Geophysical Imaging III, SPIE* **2571,** 176–186.

Wu, R. S., and X. B. Xie (1994). Multi-screen backpropagator for fast 3D elastic prestack migration, *Mathematical Methods in Geophysical Imaging II, SPIE* **2301,** 181–193.

Wu, R. S., Z. Xu, and X. P. Li (1994). Heterogeneity spectrum and scale-anisotropy in the upper crust revealed by the German continental deep-drilling (KTB) holes, *Geophys. Res. Lett.* **21,** 911–914.

Wu, R. S., S. Jin, X. B. Xie, and T. Lay (1997). Verification and applications of GSP (generalized screen propagators) method for regional wave propagation, *Proceedings of 19th Annual Seismic Research Symposium on Monitoring a Comprehensive Test Ban Treaty*, M. J. Shore, R. S. Jih, A. Dainty, and J. Erwin (Editors), 552–561.

Xie, X. B., and T. Lay (1994). The excitation of explosion Lg, a finite-difference investigation, *Bull. Seism. Soc. Am.* **84,** 324–342.

Xie, X. B., and R. S. Wu (1995). A complex-screen method for modeling elastic wave reflections, *Expanded Abstr., 65th Ann. Internat. SEG Mtg.*, 1269–1272.

Xie, X. B., and R. S. Wu (1996). 3D elastic wave modeling using the complex screen method, *Expanded Abstr., 66th Ann. Internat. SEG Mtg.*, 1247–1250.

Institute of Tectonics
University of California
Santa Cruz, California 95064
wrs@es.ucsc.edu Manuscript received 21 July 1999.